Sedimentologic, Sequence Stratigraphic and Stable Isotopic Study of the Late Cambrian Conococheague Formation, Strasburg, VA

Ruth Thompson
Advisor: Prof. A. Jay Kaufman
GEOL 394 Senior Thesis
April 30, 2003

Abstract

The Late Cambrian Conococheague Limestone near Strasburg, VA, records passive continental margin sedimentation in subtidal, peritidal and supratidal depositional environments. Various short-term cycles, recording rapid sea level changes, are preserved in the outcrop, while the overall increase in sand content of the carbonate sediments upwards in the progression provides evidence for long-term sea level regression (Koerschner and Read, 1998). A general negative-trending $\delta^{13}C$ excursion from +0.7 to -2.7‰ is recorded within the outcrop. High-resolution sampling from the lower stratigraphic section provides a constraint on combined natural and diagenetic variations across the carbonate platform. Based on lithologic, tectonic and temporal similarities, the excursion is most likely equivalent to a Sunwaptan-aged (500-495 Ma) (Palmer, 1998) negative $\delta^{13}C$ anomaly, called the HERB event, identified in Australia, Newfoundland, and western North America (Ripperdan et al., 1992; Ripperdan et al., 2002). The C isotope excursion and sea level regression occur during a period of rapid trilobite diversification, further linking strong environmental change with biological evolution. The Sr isotope composition of well-preserved limestone from the sampled outcrop suggests depositional $^{87}Sr/^{86}Sr$ of near 0.70917, which correlates with known Late Cambrian trends to an age of ~500 Ma (Montañez et al., 2000; Ripperdan et al., 1992; Ripperdan, 2002; Saltzman et al., 1998; Ebneth et al., 2001). Sulfur isotopic analyses of structurally bound sulfate in carbonates reveal ^{34}S enrichments of up to +34‰, which match other Late Cambrian bedded sulfates (Claypool et al., 1980) and carbonate associated trace sulfate (Strauss et al., 1997) recording the highest known $\delta^{34}S$ values for the Phanerozoic. Causes of the carbon and sulfur isotope excursions in the Late Cambrian Conococheague Formation and equivalents worldwide are controversial. If primary, these biogeochemical anomalies may be the result of the sudden loss of global oceanic primary productivity (Hoffman et al., 1998), widespread anoxia, and/or rapid deposition of carbonate (Varni, 2002). Given the warm global climate and high sea level, the concentration of continents at low- to mid-latitudes prior to the carbon isotope excursion likely facilitated a change in ocean circulation, which lead to a decrease in oxygen content (Knoll et al., 1996). The coupled anomalies are possibly due to water column bacterial sulfate reduction, which over time would result in ^{13}C depletion in oceanic alkalinity and ^{34}S enrichment in residual seawater sulfate.

Table of Contents

List of Figures

List of Tables

Introduction

The Cambrian Period hosted rapid biologic changes, the origins and causes of which have been greatly debated. Several theories and approaches exist. Uniformitarianists propose the rapid biological diversification could not occur without logical precursors. The apparent "explosion" at the base of the Cambrian Period appears to them due to the lack of adequate preservation (Knoll and Caroll, 1999). Neocatastrophists contend, on the other hand, that intrinsic animal evolutionary events are tied to extrinsic environmental factors. Without direct genetic evidence, paleontologists interested in Cambrian events have increasingly depended on geochemists to gain insight into the paleoclimatic, oceanographic and tectonic conditions during this time interval.

Previous research indicates that carbon and strontium isotopic compositions vary greatly during the Cambrian (Kaufman et al., 1996; Knoll and Caroll, 1999; Montanez et al., 2000; Saltzman et al., 2000). As such, Sr and C isotopes have been useful in providing a sense of timing in early animal diversification (Knoll and Caroll, 1999). For example, a large positive isotope excursion in the Late Cambrian coincides with the first occurrence of the trilobite *Glyptagnostus reticulatus* (which corresponds to the base of the Steptoean Stage) and the *Aphelaspis* Zone (Glumac and Walker, 1998). Furthermore, eighty species from the preceding *Glyptagnostus stolidotus* zone did not continue into the *G. reticulatus* zone (Saltzman et al., 2000). The peak of the Steptoean (495-490 Ma) Positive Isotopic Carbon Excursion (SPICE) takes place during the late *Dunderbergia* to early *Elvinia* trilobite biozones (Glumac and Walker, 1998; Palmer, 1998 for the Steptoean Age). Closely following this positive biogeochemical anomaly is a terminal Cambrian negative excursion, referred to as the HERB event, which coincides with conodont assemblage zone boundaries (Ripperdan et al., 1992). Specifically, the first occurrence of Sunwaptan-age diagnostic conodonts such as *Cordylodus primitivus* and *Hirsutodontus hirsutus* correspond to $\delta^{13}C$ minima (Ripperdan et al., 1992).

Although this is not a study in cladogenesis, the source of morphologic and genetic diversity (or the mechanisms driving them) through chemostratigraphic contexts establish important parameters in detailing the course of evolution through a better understanding of the carbon cycle. Animal clades radiating during the Cambrian responded to the environment by adopting ecological and biogeochemical roles they continue to assume in modern ecosystems (Knoll and Caroll, 1999). In addition, the occurrence of trilobite mass extinctions corresponds to changing environmental conditions. The positive and negative $\delta^{13}C$ excursions provide evidence for oscillation in organic carbon burial rates, and most likely, energy flow to biological communities.

Geologic Setting and Background

The Conococheague Formation records passive continental margin sedimentation during the Taconic Orogeny. The closing of the Iapetus Ocean between Laurentia and Gondwana created an island-arc basin in which carbonates preferentially precipitated (Koerschner and Read, 1998). Overlain by the Lower Ordovician Beekmantown Group and underlain by the Middle to lowermost Upper Cambrian Elbrook Limestone, the Conococheague carbonates outcrop along the fold and thrust-belt of the Valley and Ridge Province in central and southern Appalachia (Montanez and Read, 1992). Time-

equivalent formations in the southern Appalachians include the Nolichucky Shale and Copper Ridge Dolomite formations (Glumac and Walker, 1998). The formation represents subtidal, peritidal and supratidal depositional environments. Access to the outcrop used for this study can be obtained via the John Marshall Highway just outside Strasburg, VA.

The roadside outcrop preserves several subtidal to supratidal cycles reflecting sea level rise and fall in a rapidly accumulating passive margin carbonate platform. Brecciated and dolomitized exposure surfaces noted at the top of the cycles are often overlain by deep-water rhythmites suggesting rapid sea level rise. The sand content increases upwards in the formation, however, suggesting overall sea level regression during deposition of the Conococheague Formation (Koerschner and Read, 1998). Laminites with small, laterally linked hemispheroids, fine-grained rhythmites, and ribbon rock provide evidence for a deep-water, subtidal environment of deposition. Peritidal deposits are characterized by massive oolite and clastic grainstone beds, which are variably dolomitized, and occasional plate breccias. In some cases the plates appear imbricated suggesting unidirectional currents (Table 1, Fig. 1). A microbreccia with mm- to cm-sized clasts lies over the grainstones. Shallower peritidal environments contain characteristically ripple and dune cross-bedded carbonates. In quieter waters stromatolites and thrombolites (algal mats with a clotted texture) highlight the role of microbial activity in the depositional environment. Supratidal environments, where surfaces are only immersed during high tides (Prothero and Schwab, 1996), are often brecciated, slumped, or dolomitized, and some show evidence of pre-existing evaporitic minerals.

Stratigraphically above the roadside outcrop in a broad flat field on the R.L. McDonald farm, only ribs of subtidal rhythmites and ribbon rock were generally exposed at regular 25' intervals. Distances between beds were determined with a tape measure, and thicknesses calculated based on the 45^{o} angle of the dip of bedding planes. Peritidal and supratidal deposits were not exposed and may have been preferentially weathered out due to higher siliciclastic contents (Table 1). Exposed peritidal and supratidal beds were notably recrystallized (see samples JM-2-8 and JM-2-9), and some were partially dolomitized (see samples JM-2-18, JM-2-19, and JM-2-20), although none were brecciated.

Biologic indicators from time-equivalent, highly fossiliferous successions elsewhere suggest the Conococheague Formation coincide with trilobite zones located in the Dresbachian, Franconian, and Trempealeauan stages. Specifically, *Crepicephalus* and *Cedaria* of the lower Dresbachian, and *Elvinia*, *Dunderbergia*, *Prehousia*, *Dicanthopyge* and *Aphelaspis* of the upper Dresbachian (or Steptoean), and *Saukia*, *Saratogia* and *Taenicephalus* of the Franconian/Trempealeauan (or Sunwaptan) provide broad age constraints (Glumac and Walker, 1998). Accepting the known radiometric calibration of these biozones, the Conococheague may have lasted some 18 Ma (from ~523 to ~505 Ma).

Dolomite distribution shows a close relationship to regressive marine facies while the limestone corresponds with sea transgressions (Montanez and Read, 1992). Modern analogs such as the sabkha (along with composite eustacy data) provide insight into the duration of progradation and length of supratidal exposure required for dolomitization (Montanez and Read, 1992). Given the lack of bedded evaporites, however, the

conditions operating at the time of deposition more likely approximate a semi-arid environment (Montanez and Read, 1992). Hypersaline brines studied in modern environments show a wide variation in carbon isotope compositions. Causes for the variations include evaporation, precipitation of calcium carbonate, organic matter decomposition, invasion of atmospheric CO_2 and biogenic effects due to microbial deposits (Glumac and Walker, 1998). Carbonate formed in association with evaporating brines should demonstrate ^{13}C enrichment. If the ^{13}C enrichment originates from the evaporitic conditions, then coupled ^{18}O enrichment would likewise occur (Glumac and Walker, 1998).

The Late Cambrian Isotope Excursions:

Carbon and Oxygen

As previously noted, a large, positive $\delta^{13}C$ isotope excursion recorded in other sediments worldwide provides substantial insight into the perturbations of the carbon cycle during the Late Cambrian (Montanez et al., 2000; Saltzman et al., 2000). Referred to as the Steptoean (500-495 Ma) Positive Isotope Carbon Excursion (SPICE), maximum values range 4-5‰ PDB (Pee Dee Belemnite) and correlate to a craton-wide Dresbachian/ Franconian or Sauk II/Sauk III unconformity (Glumac and Walker, 1998; Palmer, 1998; Saltzman et al., 2000). This unconformity occurs during a sea level lowstand where an influx in siliciclastic material appears. Provided an increase in primary production coupled with deoxygenation of ocean basins facilitates an associated increase in organic deposition, preferential removal of light (^{12}C) carbon from the global ocean in the form of organic-rich sediments would result in the positive $\delta^{13}C$ excursion recorded (Saltzman et al., 2000). Further scientific examination of the anomaly suggests that 20-25% organic carbon was removed from the ocean at that time (Berger and Vincent, 1986).

Despite invertebrate presence during this period, fossils are rare due to diagenesis and dolotimization in carbonate sediments as well as spacing limitations in exposed beds (Glumac and Walker, 1998). Chemostratigraphy developed from previous research has therefore been used to constrain the excursion (Brasier, 1993; Saltzman et al., 2000) as the relationship between the chemostratigraphy and high-resolution samples of fossil-abundant outcrops provide strong evidence for correlation. The initial increase (-1 to +1‰) in $\delta^{13}C$ values coincides with the first occurrence of *Glyptagnostus reticulatus,* which begins at the base of the *Pterocephaliid* Biomere (Steptoean Stage), and peaks at the first occurrence of *Irvingella* (Glumac and Walker, 1998; Saltzman et al., 2000). Furthermore, eighty species from the preceding *Glyptagnostus stolidotus* zone did not proceed into the overlying *G. reticulatus* biozone (Saltzman et al., 2000). Disruption in the food chain from depletion in essential nutrients served as a catalyst in the mass extinctions (Saltzman et al., 2000). Removal of carbon from the surface ocean as a result of enhanced carbon production caused ^{12}C depletion and a decline in atmospheric pCO_2. Global cooling and extinction responses ensued (Glumac and Walker, 1998).

A coupled negative excursion (coined the HERB event) evidenced in Australia, Newfoundland, and western North America also occurs in the Late Cambrian during the Sunwaptan Stage (Ripperdan et al., 1992; Ripperdan, 2002). Although the HERB event temporally follows the positive SPICE excursion, the presence of sea level regression and

rapid trilobite diversification in both provide evidence that the two anomalies represent similar biomere patterns to different environmental factors (Ripperdan, 2002). Whereas the diversification of the *Pterocephaliid* faunas occurred during the SPICE excursion, the *Ptychaspid* fauna diversified during the HERB excursion (Ripperdan, 2002). Maximum $\delta^{13}C$ values reach -3 to -4‰ (Ripperdan et al., 1992). Causes for the negative excursion may include sea level regression, microbiolite activity and carbonate platform exposure. Weathering and erosion of the carbonate platform may have provided the source of organic carbon that drove marine $\delta^{13}C$ to negative values (Ripperdan, 2002).

Strontium

A rise in $^{87}Sr/^{86}Sr$ is also known to be associated with sea level regression and trilobite mass extinction (Montanez et al., 1996; Saltzman et al., 1998). Strontium isotopes provide information on large-scale processes such as orogenesis, climatic variations, eustacy and weathering (Montanez et al., 1996). Temporal variations are governed by changes in the interaction between riverine Sr flux to the ocean from continental weathering and hydrothermal activity at midocean ridges (Montanez et al., 1996). Peak values correlate to rapid exhumation and associated chemical weathering. The gradual decrease in the $^{87}Sr/^{86}Sr$ isotope trend following peak values represents the natural tendency for disturbed earth systems to seek equilibrium.

Strontium ratios vary little over localized segments of geologic time because the weathering and orogenic mechanisms in operation take millions of years to noticeably shift. High-order variations, if primary, imply relatively rapid (<1 Ma) changes in global seawater $^{87}Sr/^{86}Sr$, which does not correlate with the long residence time of strontium evidenced in seawater today (Ebneth et al., 2001). However, variations may arise due to radioactive decay of ^{87}Rb (Ebneth et al., 2001). As such, including rubidium in analyses provides a measure of least-altered or most primary values. The $^{87}Sr/^{86}Sr$ ratios recorded in the Conococheague support correlations with other Late Cambrian sediments, especially those associated with similar tectonic events (Montanez et al., 1996; Saltzman et al., 1995; Ebneth et al., 2001).

Sulfur

A warm global climate, high sea level and concentration of the continents at low- to mid-latitudes prior to the excursion facilitated a change in ocean circulation, which lead to a decrease in oxygen content. The anoxia preceded deposition of organic-rich sediments (Railsback et al., 1990). Sediments found in regions associated with this time interval, therefore, often contain a high degree of organic material. Previous research suggests that organic-rich, pyritic facies imply poorly oxygenated waters with stratified deeper water (Saltzman et al., 2000). The density contrasts (introduced by ocean stratification) between shallow and deep-water masses cause sluggish circulation, which also contributes to the development of anoxic conditions and would allow ^{13}C depleted alkalinity to have been formed through water column bacterial sulfate reduction (Varni, 2002; Railsback et al., 1990).

Specifically, bacterial sulfate reducers lower oceanic sulfate concentrations and oxidize organic matter. They produce both acidity (CO_2) and alkalinity (HCO_3^-) with negative isotopic compositions as well as sulfide (HS^-) concentrated in ^{32}S. Bacterial sulfate reduction relies on organisms that use low molecular weight carbon compounds to

sustain their metabolism (Habicht and Canfield, 1996; Varni, 2002). The bacterial sulfate reducers thus lower oceanic sulfate concentrations and oxidize organic matter as shown in the following reaction:

$$C_{106}H_{263}O_{110}N_{16}P + 53SO_4^{2-} \rightarrow 39CO_2 + 67HCO_3^- + 16NH_4^+ + HPO_4^{2-} + 53HS^- + 39H_2O.$$

The products are alkalinity (HCO_3^-) and acidity (CO_2) with negative isotopic compositions as well as sulfide (HS^-), concentrated in ^{32}S (Varni, 2002). As a result, the residual pool of oceanic sulfate (the left hand side of the equation) becomes enriched in ^{34}S. It is important to note, however, that this reaction depends on the availability of iron, which would combine with the HS^- to precipitate out of the system as insoluble pyrite Fe_2S (Varni, 2002).

From 700 Ma to the Cambrian/Precambrian boundary, a positive sulfur anomaly, known as the Yudomski Event, demonstrates a possible rapid enrichment up to +25 to +30‰ (Holser et al., 1989). Sulfur isotopic analyses of structurally bound sulfate in carbonates have also been reported as ^{34}S enrichments of up to +34‰, which also match other Late Cambrian bedded sulfates (Claypool et al., 1980) and carbonate associated trace sulfate (Strauss et al., 1997) In contrast, modern rivers deliver sulfur on the order of +6 to +10‰ (Varni, 2002).

Sampling Strategy and Investigative Methods

In order to obtain high-resolution stratigraphic samples, the length of the roadside outcrop was measured in detail with Dr. Kaufman and University of Maryland graduate student Craig Hebert. Rock types, sedimentary features, grain size distributions, and probable depositional environments, as well as the position of exposure and maximum flooding surfaces were recorded. Starting at the base of the outcrop and working up-section, samples were collected from each bed for approximately 25 m, and thereafter at ~0.5 m intervals (Table 1, Fig. 1).

Samples were labeled and placed into Gladlock plastic bags. Slabs of rock samples (<2.5cm width) were made by using a lapidary trim saw. Each specimen was carefully inspected to ensure that cross-sections were adequately represented. Slab surfaces were then ground to a high polish using the Struers Labopol grinding apparatus. Coarse grit sand paper (grade 80) was used on first pass to smooth out the rougher edges caused by the trim saw blade. Finer grit sand paper (grade 320) finished the surfaces prior to microdrilling (Fig. 2a-d).

Cathodoluminescence Observations

In order to avoid obtaining data from diagenetic zones, carefully chosen fine-grained textures were identified visually and through cathodoluminescence (CL) observation to extract carbonate powder from least-altered areas. Operating conditions for the CL are reported in Table 2. CL is a useful tool for studying meteoric diagenesis of marine carbonates insofar as fresh waters are variably enriched in manganese, the element typically responsible for luminescence in carbonates, relative to seawater. Thus, areas with high illumination prove undesirable. Photographs taken using cathodoluminescence illustrate the compositional variations in carbonate and siliciclastic

textures (Fig. 3a-d). Cathodoluminescence (CL) analyses were performed on four samples (JM-1-100, JM-2-0, JM-2-2, and JM-2-25) based on their lithology as well as their distribution within the stratigraphic column; three peritidal microbialaminites and one subtidal ribbon rock. Samples were dried in the laboratory oven at 90°C in order to expel water vapor, which would have interfered with the CL scope.

Sample Isolation

The results of the petrographic and CL examinations were used to determine the least altered part of the sample on the polished thick section, which was microdrilled with a 1.0 mm diamond studded drill bit (to a depth of no greater than 4 mm) on a Servo Products drill press, for subsequent isotopic analyses. The finest-grained and least luminescent zones were chosen for microdrilling. The resulting powder was transferred into labeled small plastic containers for C, O, and Sr isotopic analyses. These extra measures were taken despite contrary evidence suggesting that diagenesis does not significantly affect carbon isotopic results (Kaufman et al., 1991).

Carbon and Oxygen Isotope Analyses

Wheaton V reaction vials were prepared by rinsing them in milliQ water and boiling in nitric acid for one hour. The vials were then sonicated for twenty minutes and dried overnight in the laboratory utility oven. Following cleaning, 200-400 μg of powdered sample were transferred to the Wheaton V reaction vials. The vials were sealed with blue septa and Kel-F teflon discs to prevent atmospheric leaks. A pure carbonate house standard powder (LL1) was measured repeatedly in each run to determine the external precision of sample analyses. Calibrated values for $\delta^{13}C$ and $\delta^{18}O$ for LL1 are +1.0 and -10.5‰, respectively, vs. VPDB. Carbonates were acidified with phosphoric acid on a MultiPrep device and resulting CO_2 transferred to the dual inlet of the IsoPrime mass spectrometer for isotopic analysis. Phosphoric acid reacts with the carbonate powder to produce CO_2. The CO_2 is measured and analyzed in the mass spectrometer for $\delta^{13}C$ and $\delta^{18}O$. The original phosphoric acid purchased contains 85% acid and 15% water. In order to avoid complications that might arise from extra oxygen reacting with carbonate powder, the water is driven off by addition of phosphorous pentoxide (P_2O_5), which supersaturates the solution with respect to PO_4^{2-}. The concentration of the acid is verified by checking its density, which should fall between 1.89-1.92 g/ml.

The raw sample results for each run were corrected based on the average of 10 LL1 standards in each run. The daily offset from the true value of the LL1 standards was applied to raw sample values. The standard deviations shown in Table 3 represent 1σ and 2σ uncertainties.

Strontium Separation and Isotope Analyses

Samples were pretreated by adding 1-1.5 ml of 0.2M ammonium acetate to 1-3 mg of microdrilled carbonate powder in a microcentrifuge tube. The sample was shaken and allowed to leach for 30 minutes, then centrifuged for 5 minutes. The supernatant was removed and stored in a clean 5 ml Teflon vial. These steps were repeated three times. Leached samples were dissolved with 1 ml of 0.5M acetic acid and left to react overnight;

they were then centrifuged for 5 minutes and the supernatant removed and stored in 5 ml Teflon vials. Samples were subsequently dried on a hot plate in a clean environment.

When the sample completely dried, Sr-Spec resin was loaded with a 1 ml pipette tip into chromatographic micro-columns. The resin was prepared by rinsing with 4 RBV (resin bed volume) 3M HNO_3. The sample was then loaded in 1-6 RBV 3M HNO_3 and passed through the column to collect REE. Next, 2 RBV 3M HNO_3 was passed through the column to collect REE. When 6 RBV 7M HNO_3 passed through, however, it was discarded. Likewise, 1 RBV 3M HNO_3 was added and discarded. Finally, 4 RBV 0.05M HNO_3 was passed through and Sr collected. The sample then dried on a hot plate in a clean, fumigated environment.

The isolated Sr collected was split in half and mounted on a Re filament treated with 1 µl TaO and dried under current. Samples were analyzed between 1550-1650° C on a VG 54 multi-collector thermal ionization mass spectrometer (TIMS) at the University of Maryland, which is standardized to NBS-987 with an accepted value of 0.710235 +/- 0.000039 for 2σ. The beam was set between 0.5 and 1 volt such that greater than 50 ratios could be collected (Table 5).

Trace Sulfate Extraction

Carbonate-associated sulfate concentrations were determined using a method developed at the University of Missouri, which was modified from Burdett et al. (1998) and detailed in University of Maryland graduate student Mike Varni's thesis (Varni, 2002). Between 65-100g of sample was crushed with a Spex 8500 Shatterbox to produce the fine powder. Between each sample, the ceramic ring and puck were cleaned with quartz chips and washed with 200% ethanol. The five chosen samples, JM-1-40, JM-1-5, JM-1-75, JM-1-4 and JM-1-66, were transferred to one-liter beakers and treated with double distilled water for 24 hours, stirring occasionally. Massive grainstones JM-1-5 and JM-1-40 represent peritidal environments; stromatolitic JM-1-75 represents supratidal deposition; micritic JM-1-4 and JM-1-66 represent the subtidal facies. After the initial 24 hours, the water was decanted and the process repeated for an additional 24 hours to remove any soluble sulfate from the sample. The samples were then treated with a 5.25% solution of NaClO for 24 hours. This step removes any organic matter, organically-bound sulfate, residual soluble sulfates, and metastable sulfides, which would obscure data pertaining to the structurally bound sulfate in the carbonates. The samples were again decanted, treated with milliQ water and allowed to sit overnight. Samples were then decanted after the remaining carbonate material had settled, and dissolved with 3M HCl. Once the reaction between the carbonate and HCl stopped and the solutions sat for 24 hours, the samples were filtered. The unreacted material was saved to determine the amount of insoluble residue. The solutions were filtered with a 0.45 µm micropore system to remove any micro-particulates. The sulfate precipitated as barium sulfate ($BaSO_4$) by adding 60-80ml of saturated 30% $BaCl_2$ solution. The sample was heated to near boiling for several minutes to facilitate precipitation. After removing from heat and letting them to cool for a few minutes, the samples were covered and left for 2-3 days to allow the reaction to proceed. Barium sulfate precipitates were isolated using a similar micropore system to the one previously mentioned and 0.45 µm HVLP filters. Once the precipitate dried, the barium sulfate was scraped off for analysis in a continuous flow

(CF) gas source Isoprime mass spectrometer with a Eurovector combustion and chromatographic interface.

Data Presentation

Table 1.
Stratigraphy

Sample	Total Feet	Total Meters	Lithology
JM-2-25	1427.8	435.2	Ribbon rock
JM-2-24	1402.8	427.6	Ribbon rock
JM-2-23	1340.8	408.7	Ribbon rock (?)
JM-2-22	1315.8	401.1	
JM-2-21	1277.8	389.5	Nodular grainstone
JM-2-20	1217.8	371.2	Grainstone, partially dolomitized
	1150.8	350.8	Pre-existing carbonate grains
JM-2-19	1150.3	350.6	Grainstone, with some dolomitization
JM-2-18	1125.8	343.1	Grainstone, with some dolomitization
JM-2-17	1071.8	326.7	
JM-2-16	1023.3	311.9	Nodular, bedded grainstone
JM-2-15	965.3	294.2	More wavy ribbon rock, making it look nodular
JM-2-14	890.3	271.4	Rhythmite ribbon rock, finely laminated, flat
JM-2-13	831.3	253.4	Wavy, nodular limestone
JM-2-12	756.3	230.5	Nodular, sandy limestone
JM-2-10	731.3	222.9	Grainstone w/hint of x-bed; exposure surface above
JM-2-11	663.3	202.2	More sandy, more shallow microbial laminite
JM-2-9	622.3	189.7	Granularite w/some x-beds; sugary texture, veining due to recrystallization (fluids flowing thru hi sand content)
JM-2-8	597.3	182.1	Massive, sandy (w/recrystallization)
JM-2-7	572.3	174.4	Nodular ribbon rock, subtidal EOD
JM-2-6	522.3	159.2	Rhythmite to ribbon rock
	507.3	154.6	Massive limestone
JM-2-5	506.8	154.5	Nodular ribbon rock, subtidal EOD
JM-2-4	256.8	78.3	Ribbon rock
JM-2-3	219.8	67	
JM-2-2	197.8	60.3	Laminite
JM-2-1	155.8	47.5	Flat-laminated
JM-2-0	132.3	40.3	More shallow EOD (than previous bed)
JM-1-100	127.3	38.8	Microbial laminite
Precise measuring resumes			
JM1-83	78.3	23.9	
JM1-82	77.3	23.6	
JM1-78	76.3	23.3	
JM1-75b	75.3	23	microbial laminite, stromatolite
JM1-74	74.3	22.6	Breccia

JM1-73	73.3	22.3	Breccia
JM1-72	72.3	22	Stromatolite
JM-1-68	71.3	21.7	Stromatolite
JM-1-67	70.3	21.4	massive grainstone with mud clasts
JM-1-66	69.3	21.1	Grainstone
			ribbon rock, subtidal EOD
JM-1-64	68.3	20.8	disturbed section
JM-1-62	67.3	20.5	partially dolomitized micrite
JM-1-60	66.3	20.2	exposed surface, evaporated layer, transition to next cycle
JM-1-59	65.3	19.9	stromatolitic, cherty
exact measurements not taken from here on up, samples obtained at ~1 foot intervals			
JM-1-58	64.3	19.6	thrombolitic, clotted
JM-1-57			brecciated, base of next cycle
JM-1-44	50.6	15.4	organic-rich, massive grainstone
JM-1-43, JM-1-40	47.6	14.9	massive grainstone
JM-1-38	46.6	14.5	stromatolitic, microbial laminite
	45.8	14.2	Grainstone
JM-1-35	43.3	13.9	deeper water ribbon rock with some breccia, subtidal EOD
	41.1	13.2	platy breccia
JM-1-33	40.8	12.5	transitioning: microbial laminite with small, laterally-linked hemispheroids into cross-bedded layer into fine-grained
		12.4	rhythmite (possible MFS)
JM-1-25	38.7		grainstone, carbonate clasts, sand grains, wavy texture, cross-beds, high energy
		11.8	soft sediment deformation, mudchips, shallow EOD
	31.7		stromatolitic, microbial layered mound
JM-1-19	30.3	9.7	low angle cross-beds, carbonate clasts, weathered-out mudchips at top of bed
JM-1-17	27.3	9.2	Brecciated
JM-1-15	24.3	8.3	cross-bedded layer with longer currents, possible dunes (?)
	20.7	7.4	thrombolitic grainstone, "clotted" texture, pref. dolomitized
JM-1-13	18.6	6.3	
JM-1-12	18.2	5.7	variegated limestone with clear cross-bedding, 1st evidence of current activity
		5.5	
	16.7		grainstone with occasional oolites, some contorted beds
	16.2	5.1	microbreccia with mm- to cm-sized clasts
	15.7	5	oolite with mudchips and smaller ooids
JM-1-9	13.4	4.8	fine-grained grainstone
JM-1-7	12.2	4	massive oolite with mudchips
JM-1-5	8.8	3.7	fine-grained grainstone
JM-1-4	4.7	2.7	micrite/dolomicrite
	3.3	1.4	platy breccia w/lighter dolomitic clasts, sense of imbrication
	2.3	1	vermicular, "wormy" grainstone
	1.3	0.7	dolomitic micrite
JM-1-0	0	0	basal breccia w/rip-up clasts, peritidal, high energy EOD

Figure 1. Stratigraphic Column

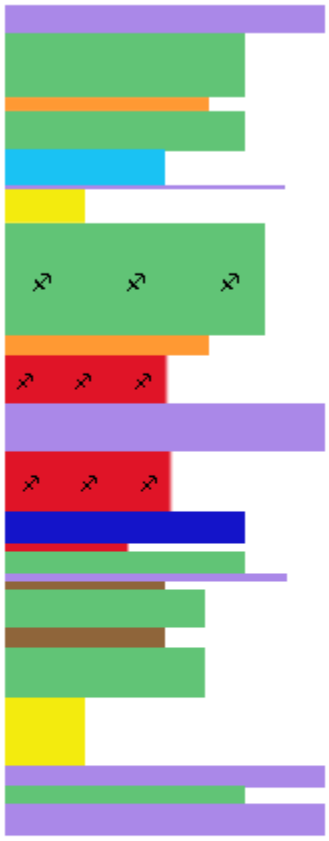

Massive, organic-rich

Exposure surface, bottom of cycle, prior to grainstone

Ribbon rock with some breccia

Rhythmite laminite, possible MFS

Carbonate clasts, x-beds, soft sediment deformation, sand grains, mudchips followed by microbial laminite with small, laterally-linked hemispheroids

Low angle x-beds, weathered-out mudchips at top, carbonate clasts, ↗

X-beds with longer currents, possible dunes (?), ↗
Clotted texture
Variegated with clear x-beds, ↗
Occasional ooids, contorted bedding
Microbreccia with mm- to cm-size clasts
Oolite with mudchips and smaller ooids

Massive oolite with mudchips

Platy breccia with lighter dolomitic clasts and a sense of imbrication
Vermicular grainstone **cs**
Basal breccia with rip-up clasts

Legend:
light purple - breccia
green - grainstone
yellow - micrite
brown - oolite
dark blue - thrombolite
red - limestone
orange - stromatolite
light blue - ribbon rock
↗- cross-bedding
cs- vermicular

Scale: 3 mm = 1 foot or 0.3048 m

Figure 2(a-d): Polished Slabs

JM-1-83 Micrite

JM-1-57 Breccia

JM-1-14 Grainstone

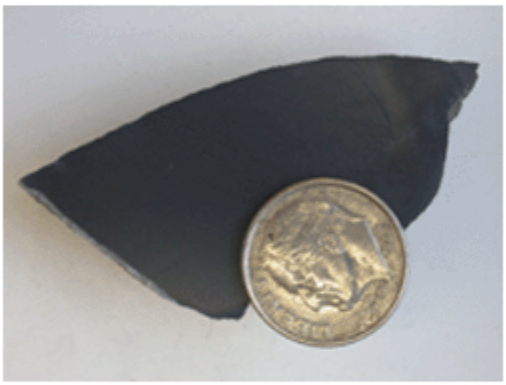

JM-1-35 Ribbon rock w/ some breccia

JM-1-44 Grainstone

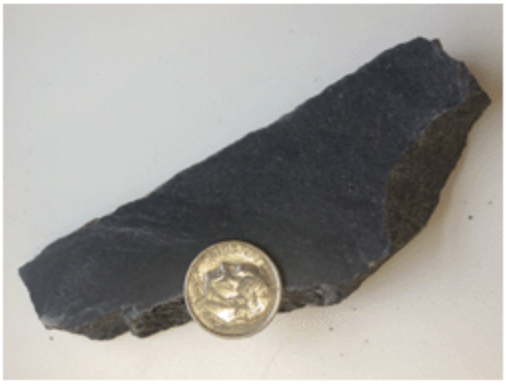

JM-1-7 Massive oolite with mudchips

Table 2. Cathodoluminescence Data

Sample	mtorr	Milliamps	Kv	focus	Lithology
JM-1-100	100	17.5	8	80	microbial laminite
JM-2-0	105	15	7.5	70	more shallow laminite
JM-2-2	105	15	7.5	75	Laminite
JM-2-25	105	15	7.5	70	ribbon rock

Figure 3(a-d): Photospectrometry (drill hole = 1 mm diameter)

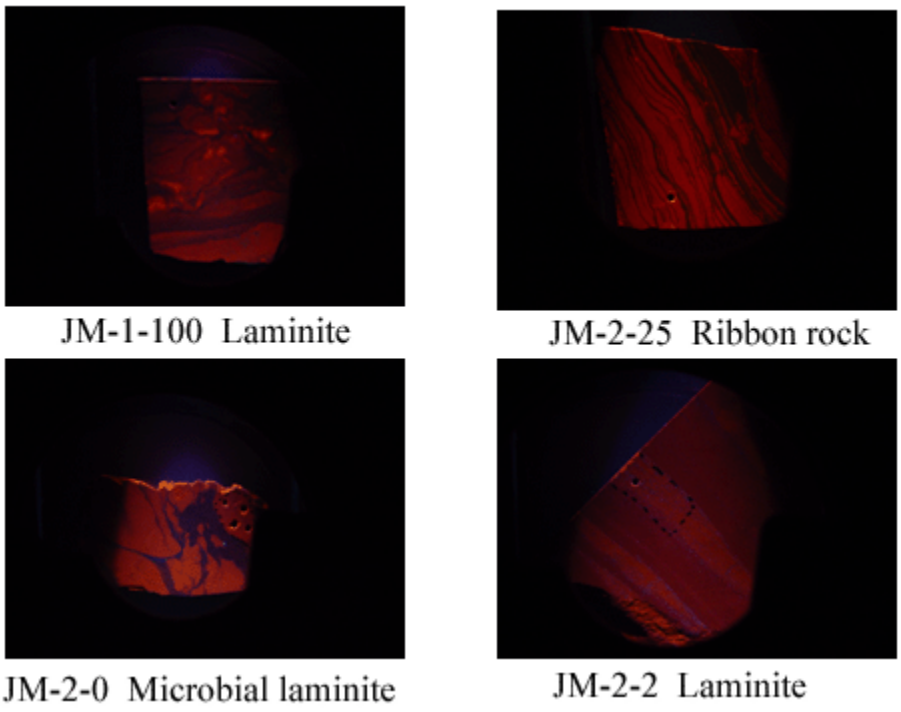

JM-1-100 Laminite

JM-2-25 Ribbon rock

JM-2-0 Microbial laminite

JM-2-2 Laminite

Table 3. Carbon Isotope Data (LL1 Standards)

Sample #	δ13C	std error	δ18O	std error
Run 1a				
LL1-473	0.296	0.002	-10.172	0.007
LL1-474	0.524	0.002	-9.933	0.006
LL1-475	0.535	0.002	-9.938	0.004
LL1-476	0.447	0.001	-10.13	0.009
LL1-477	0.444	0.003	-10.124	0.005
LL1-478	0.488	0.004	-10.163	0.002
LL1-479	0.504	0.002	-10.132	0.005
LL1-480	0.546	0.002	-10.087	0.002
LL1-481	0.487	0.007	-10.179	0.006
LL1-482	0.468	0.005	-10.322	0.01
Avg	0.494		-10.112	
std dev	0.037		0.12	
2σ	0.074		0.24	

Adjusted LL1 Values (Run1a)

δ13C	δ18O
0.506	-0.388

Run 1b				
LL1-483	0.482	0.003	-10.48	0.005
LL1-484	0.549	0.003	-10.26	0.008
LL1-485	0.465	0.004	-10.393	0.005
LL1-486	0.497	0.002	-10.34	0.004
LL1-487	0.549	0.006	-10.194	0.006
LL1-488	0.498	0.005	-10.368	0.008
Avg	0.507		-10.339	
std dev (1σ)	0.035		0.101	
2σ	0.07		0.202	

Adjusted LL1 Values (Run 1b)

δ13C	δ18O
0.493	-0.161

Run 2				
LL1-764	0.764	0.003	-9.456	0.003
LL1-765	0.752	0.006	-9.396	0.011
LL1-766	0.737	0.004	-9.41	0.006
LL1-767	0.773	0.004	-9.43	0.005
LL1-768	0.761	0.004	-9.379	0.005
LL1-769	0.792	0.003	-9.384	0.005
LL1-770	0.783	0.002	-9.448	0.003
LL1-771	0.76	0.004	-9.401	0.009
LL1-772	0.75	0.002	-9.446	0.007
LL1-773	0.739	0.003	-9.473	0.009
Avg	0.761		-9.423	
std dev (1σ)	0.018		0.033	

Adjusted LL1 Values

δ13C	δ18O

2σ	0.036		0.066		0.239	-1.077
Run 3						
LL1-868	0.675	0.003	-9.645	0.009		
LL1-870	0.663	0.004	-9.494	0.011		
LL1-871	0.648	0.006	-9.602	0.01		
LL1-872	0.714	0.004	-9.511	0.009		
LL1-873	0.701	0.004	-9.444	0.006		
LL1-874	0.724	0.002	-9.484	0.006		
LL1-875	0.706	0.002	-9.447	0.009		
LL1-876	0.712	0.002	-9.45	0.005		
LL1-877	0.712	0.003	-9.464	0.004	**Adjusted LL1 Values (Run 3)**	
					δ13C	**δ18O**
Avg	0.695		-9.505		0.305	-0.995
Std dev (1σ)	0.026		0.072			
2σ	0.052		0.144			

Table 4a.
Carbon Isotope Data

Sample #	**δ13C**	**std error**	**δ18O**	**std error**		**δ13C (corr)**	**δ18O (corr)**
JM1-0	0.73	0.005	-8.567	0.005	**Run 1**	1.236	-8.955
JM1-2	0.34	0.005	-9.422	0.007		0.846	-9.81
JM1-4	0.724	0.007	-8.384	0.008		1.23	-8.772
JM1-5	0.469	0.003	-8.665	0.007		0.975	-9.053
JM1-7	0.42	0.005	-9.26	0.006		0.926	-9.648
JM1-9	0.69	0.003	-8.969	0.008		1.196	-9.357
JM1-12	0.089	0.003	-9.967	0.006		0.595	-10.355
JM1-13	-0.054	0.005	-10.068	0.006		0.452	-10.456
JM1-14	0.218	0.007	-9.645	0.006		0.724	-10.033
JM1-15	0.298	0.005	-9.616	0.002		0.804	-10.004
JM1-17	0.161	0.003	-9.848	0.005		0.667	-10.236
JM1-20							
JM1-25	0.244	0.008	-9.734	0.006		0.75	-10.122
JM1-33	0.262	0.007	-8.087	0.009		0.768	-8.475
JM1-35	0.093	0.009	-9.874	0.011		0.599	-10.262
JM1-38x	-1.472	0.008	-9.94	0.01		-0.966	-10.328
JM1-38y	-1.46	0.007	-9.886	0.008		-0.954	-10.274
JM1-40	0.128	0.005	-9.573	0.004		0.634	-9.961
JM1-43	-0.016	0.006	-9.578	0.006		0.49	-9.966
JM1-44	-0.492	0.007	-9.43	0.007		0.014	-9.818
JM1-58a	0.63	0.004	-8.813	0.006		1.136	-9.201
JM1-58b	0.199	0.005	-9.583	0.007		0.705	-9.971
JM1-59	0.493	0.005	-8.226	0.012		0.999	-8.614
JM1-60	-0.477	0.004	-9.588	0.008		0.029	-9.976
JM1-62	-0.003	0.005	-9.628	0.006		0.503	-10.016
JM1-64	-0.174	0.008	-8.951	0.009		0.332	-9.339

JM1-66	-1.179	0.004	-9.766	0.009		-0.673	-10.154
JM1-67	-0.607	0.011	-10.113	0.012		-0.101	-10.501
JM1-68	-0.081	0.004	-9.457	0.005		0.425	-9.845
JM1-69	-0.538	0.004	-9.427	0.01		-0.032	-9.815
JM1-72	-1.039	0.007	-10.068	0.013		-0.533	-10.456
JM1-73	-1.378	0.006	-9.545	0.007		-0.885	-9.706
JM1-74	-1.11	0.006	-9.68	0.009		-0.617	-9.841
JM1-75a	-0.795	0.004	-8.654	0.008		-0.302	-8.815
JM1-75b	-1.133	0.005	-8.94	0.003		-0.64	-9.101
JM1-78	-1.249	0.005	-9.7	0.004		-0.756	-9.861
JM1-82	-0.242	0.005	-9.18	0.006		0.251	-9.341
JM1-83	0.657	0.002	-8.661	0.001		1.15	-8.822
JM1-100	0.204	0.002	-8.127	0.005	**Run 3**	0.509	-9.122
JM2-0	-0.483	0.002	-8.266	0.005		-0.178	-9.261
JM2-1	0.276	0.005	-8.434	0.005		0.581	-9.429
JM2-2	0.164	0.004	-8.198	0.007		0.469	-9.193
JM2-3	-0.033	0.002	-8.241	0.008		0.272	-9.236
JM2-4	-0.282	0.009	-7.809	0.004		0.023	-8.804
JM2-5	-1.507	0.002	-7.069	0.007		-1.202	-8.064
JM2-6	-0.921	0.004	-7.616	0.005		-0.616	-8.611
JM2-7	-0.611	0.005	-8.278	0.008		-0.306	-9.273
JM2-8	-0.032	0.004	-7.745	0.008		0.273	-8.74
JM2-9	-0.935	0.003	-7.746	0.005		-0.63	-8.741
JM2-10	-2.754	0.002	-9.277	0.015		-2.449	-10.272
JM2-11	-1.932	0.003	-8.962	0.006		-1.627	-9.957
JM2-12	-2.468	0.003	-8.969	0.004		-2.163	-9.964
JM2-13	-2.051	0.004	-8.234	0.008		-1.746	-9.229
JM2-14	-1.824	0.008	-8.143	0.018		-1.519	-9.138
JM2-15	-1.014	0.002	-8.124	0.008		-0.709	-9.119
JM2-16	-0.156	0.008	-8.35	0.009		0.149	-9.345
JM2-17	-1.456	0.003	-8.653	0.005		-1.151	-9.648
JM2-18	-1.589	0.004	-8.522	0.008		-1.284	-9.517
JM2-19	-0.754	0.005	-8.498	0.009		-0.449	-9.493
JM2-20	0.071	0.004	-6.694	0.011		0.376	-7.689
JM2-21	-1.618	0.004	-8.474	0.008		-1.313	-9.469
JM2-22	-2.217	0.004	-7.986	0.006		-1.912	-8.981
JM2-23	-2.201	0.008	-6.624	0.011		-1.896	-7.619
JM2-24	-1.335	0.004	-8.593	0.003		-1.03	-9.588
JM2-25	-2.197	0.004	-9.273	0.01		-1.892	-10.268

Table 4b.
Reproducibility

Sample #	Run 2		Run 2 (Corr)	
	δ13C	**δ18O**	**δ13C**	**δ18O**
JM1-0	0.782	-8.447	1.021	-9.524
JM1-4	0.908	-7.78	1.147	-8.857
JM1-5	0.645	-8.018	0.884	-9.095
JM1-7	0.664	-8.658	0.903	-9.735
JM1-12	0.527	-9.07	0.766	-10.147
JM1-13	0.265	-9.303	0.504	-10.380
JM1-14	0.38	-8.924	0.619	-10.001
JM1-15	0.76	-8.646	0.999	-9.723
JM1-17	0.452	-9.065	0.691	-10.142
JM1-20	0.635	-8.699	0.874	-9.776
JM1-25	0.472	-8.924	0.711	-10.001
JM1-35	0.465	-9.011	0.704	-10.088
JM1-38	-1.005	-8.992	-0.766	-10.069
JM1-40	0.377	-8.814	0.616	-9.891
JM1-43	0.17	-8.792	0.409	-9.869
JM1-58a	0.956	-7.889	1.195	-8.966
JM1-58b	0.512	-8.775	0.751	-9.852
JM1-59	0.667	-7.39	0.906	-8.467
JM1-60	-0.153	-8.709	0.086	-9.786
JM1-62	0.194	-8.946	0.433	-10.023
JM1-64a	0.484	-7.588	0.723	-8.665
JM1-64b	0.525	-7.378	0.764	-8.455
JM1-68x	-0.211	-9.628	0.028	-10.705
JM1-68b	-0.7	-9.253	-0.461	-10.330
JM1-69	-0.351	-8.95	-0.112	-10.027
JM1-72	-0.377	-8.749	-0.138	-9.826
JM1-73	-1.246	-8.852	-1.007	-9.929
JM1-74	-0.864	-8.819	-0.625	-9.896
JM1-75a	-0.688	-8.046	-0.449	-9.123
JM1-78	-0.956	-8.764	-0.717	-9.841
JM1-82	-0.223	-8.806	0.016	-9.883
JM1-83	0.559	-8.523	0.798	-9.600

Fig. 4 - Distance vs. Carbon and Oxygen Isotopes with Stratigraphic Column

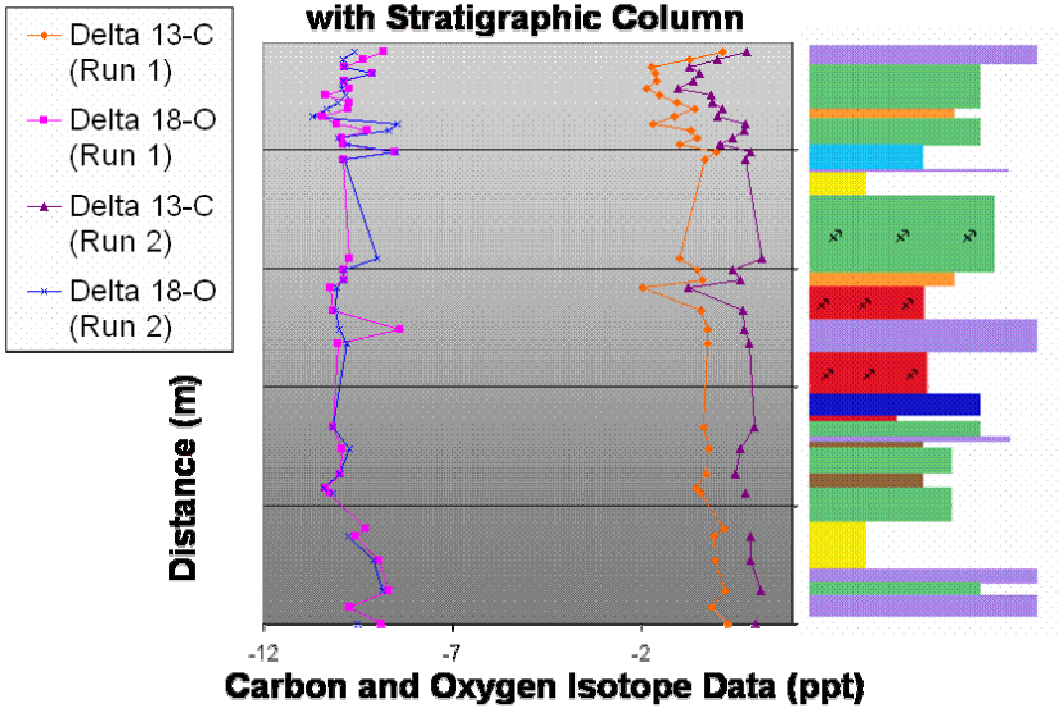

Fig. 5 Carbon and Oxygen Isotopes

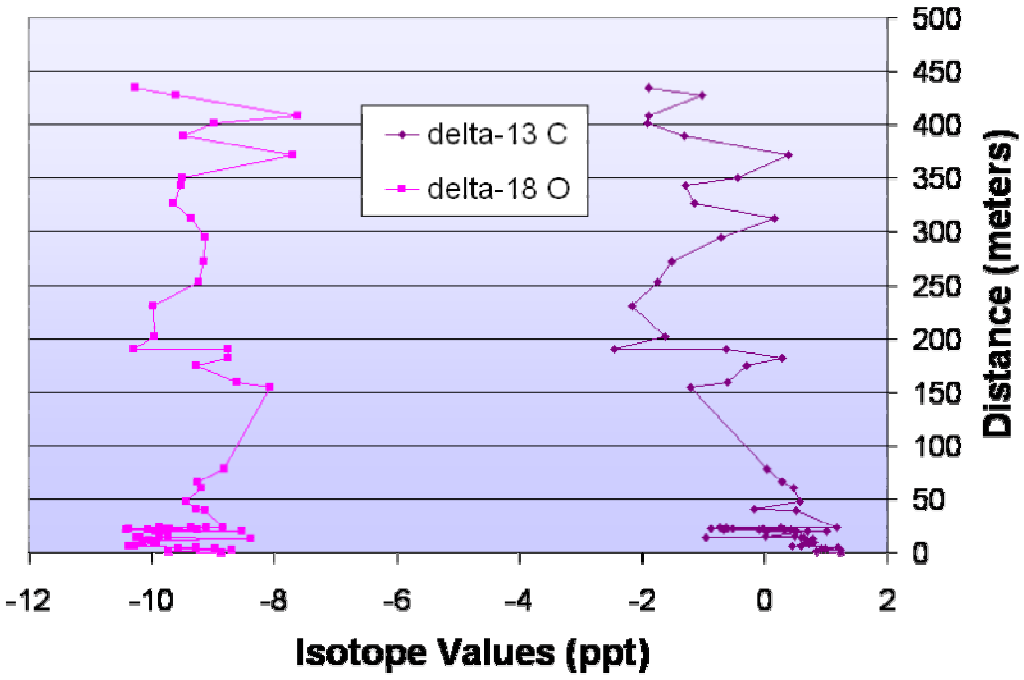

Table 5. Strontium Isotope Data

Sample	86/88	87/86	84/86	Rb (ppm)	85Rb/86Sr	Ratios	
SRM 987	0.119265	0.710268	0.056518	25.836	0.000048	93	
	0.120161	0.710234	0.056541	1794.064	0.0033253	94	
	0.119970	0.710235	0.056528	181.266	0.0003355	95	
JM-1-44	0.119677	**0.709170**	0.056506	**263.273**	**0.0004871**	96	
JM-1-33	0.119880	0.709619	0.056722	2804.215	0.0051991	8	
	0.118888	0.709736	0.056668	1025.843	0.0019073	37	
JM-1-75b	0.118909	0.709495	0.056599	319.974	0.0005944	68	
	0.119431	0.709370	0.056601	372.092	0.0006894	73	
JM-1-66	0.118921	0.709533	0.056747	2361.595	0.0044033	29	
	0.119673	0.709491	0.056465	571.59	0.0010583	69	
JM-1-9	0.118456	0.709665	0.057137	4403.038	0.0082322	10	
	0.119797	0.709556	0.056545	1033.829	0.0019148	19	Low intensity
	0.118665	0.709491	0.056537	620.259	0.0011537	10	hi intensity

The red text highlights the lowest Rb correction for each sample. JM-1-44 shows the lowest Rb correction, and is therefore chosen as the most primary 87Sr/86Sr value.

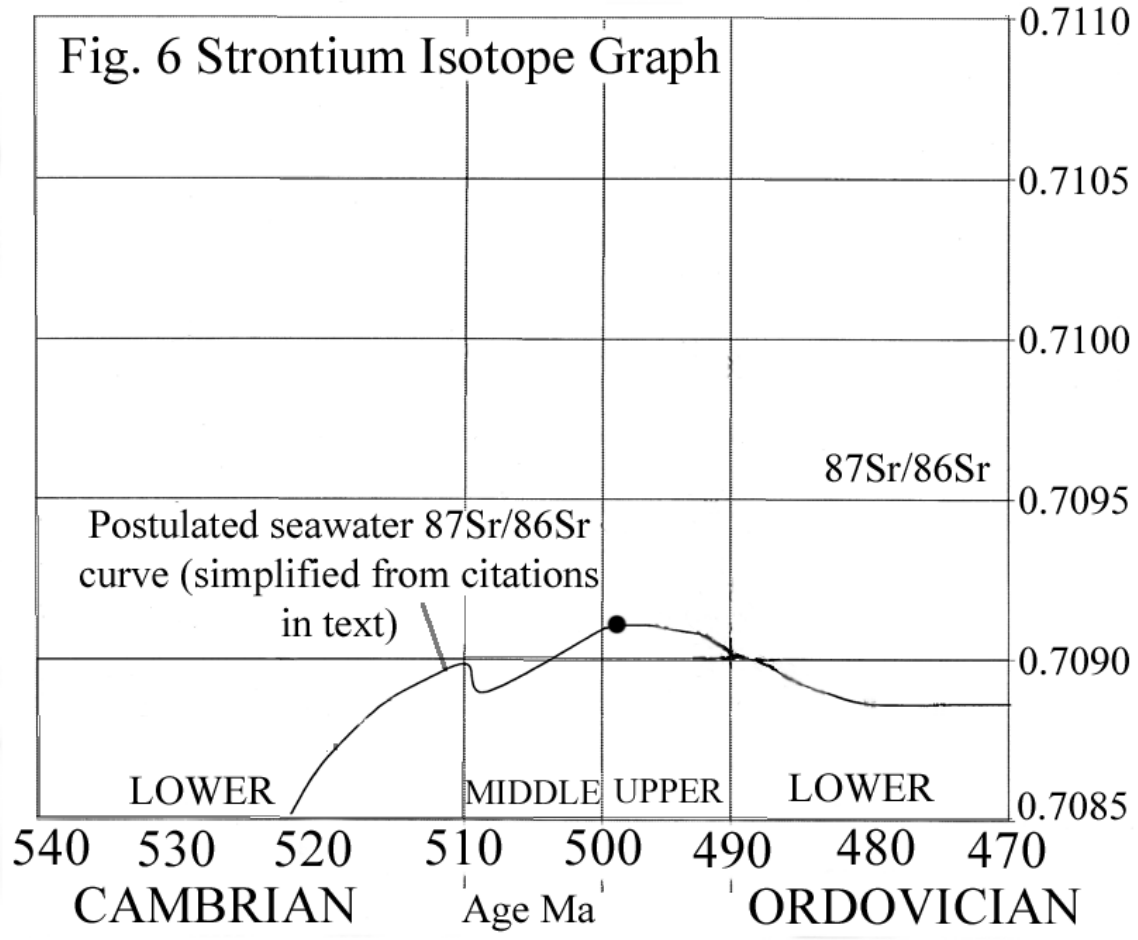

Artistic rendition after Ebneth et al., 2001
Black dot represents primary $^{87}Sr/^{86}Sr$ recorded in Conococheague carbonates, which correlates to 500 Ma in conjunction with tectonic and latitude similarities characteristic with other Late Cambrian sediments worldwide (Ebneth et al., 2001; Montañez et al., 2000; Saltzman et al., 1998).

Table 6. Sulfur Isotope Data

Standard		RT (sec)	Height (nA)	δ 34S
1276		82.5	1.33	26.05
1277		83	1.53	25.25
127a		82.8	0.73	22.77
127b		84.5	0.41	18.98
127c		83.8	0.51	20.17
Avg				20.64

Sample	Strat #	RT (sec)	Height (nA)	δ34S
RT1	JM-1-5	83.8	0.27	33.06
R2	JM-1-75	83.9	0.46	18.26
RT3	JM-1-66	82.2	0.27	33.06
R4	JM-1-40	84.3	0.37	26.23
RT5	JM-1-4	83.3	0.39	34.39

Prior to analyzing the trace sulfate, the mass spectrometer experienced repeated technical difficulties. As such, the uncertainty of the data cannot be ignored. However, the standard should read approximately 21.0 and 127a-c reflect values within a reasonable amount; these measurements have thus been averaged and compared to the data obtained for the Conococheague samples. This assumption also coincides with previously published data of +30 to +35‰ $\delta^{34}S$ enrichment in other Late Cambrian sediments (Claypool et al., 1980; Strauss et al., 1997).

Figure 7. A Geochemical Model of Late Cambrian C and S Isotope Excursions

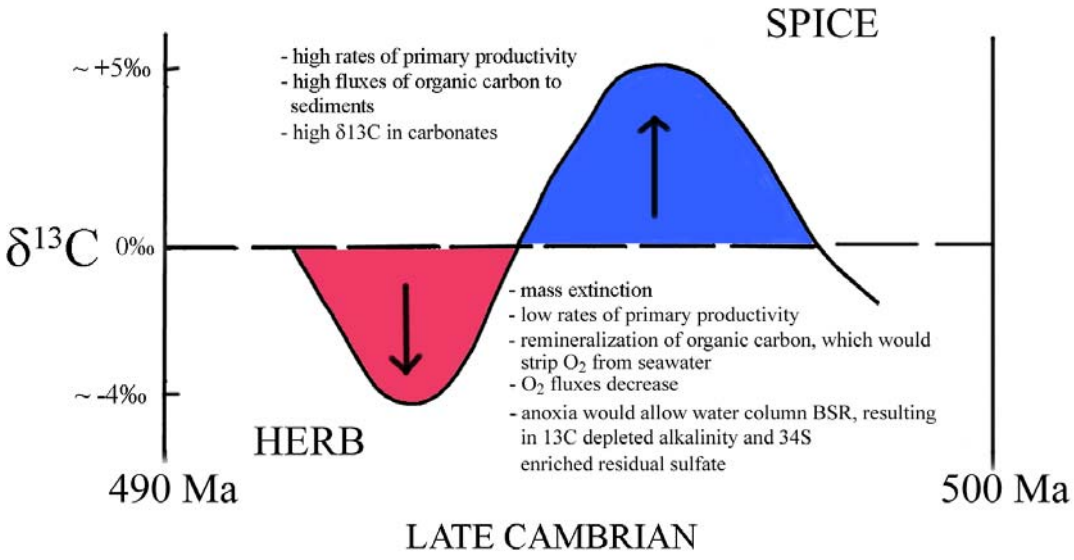

Discussion of Results and Error Analysis

Prior to evaluating the stratigraphic importance of isotope variations in the Conococheague Formation, the degree of natural or diagenetic variability must be assessed. To this end, petrographic (cathodoluminescence), geochemical (oxygen and strontium isotopes), and stratigraphic (carbon isotopes) tests were used.

CL Observations

Cathodoluminescent photospectrometry is a useful tool in studying meteoric diagenesis of marine carbonates insofar as fresh waters are variably enriched in manganese, the element responsible for luminescence, relative to seawater. Areas with high illumination thus prove undesirable.

Some of the carbonate textures from the Conococheague displayed moderately luminescent zones. However, variations in luminescence were found to be additionally related to the amount of siliciclastic material present in the fine-grained carbonates. The application of HCl to carbonate textures highlighted zones of silica abundance, which corresponded the more luminescent areas observed with the CL scope.

As a result, only non-luminescent carbonate rich textures were chosen for isolation and analysis. The ribbon rock (i.e., sample JM-2-25 with 1 mm drill hole for scale) photographed demonstrates clear areas of dark carbonate and further supports the premise that the subtidal beds represent least-altered, most primary carbonate values (Figure 3b).

Oxygen Isotopes

Oxygen isotopic compositions of the carbonates range between -7.619 and -10.456‰ (Table 4a). There is a notable lack of oxygen isotope variability, suggesting good overall preservation insofar as oxygen isotopes are sensitive indicators that decrease with increased alteration (Varni, 2002). These values are also consistent with well preserved Late Cambrian carbonates worldwide (Montañez et al., 2000; Saltzman et al., 1998).

The lack of covariance between carbon and oxygen isotopes further suggests that diagenesis was not as significant a factor in producing the values obtained as seasonal variations. While $\delta^{13}C$ values progress from 0.223 ‰, -0.032 ‰, -0.081 ‰ to 0.189 ‰ between 1.4m and 4.0m corresponding $\delta^{18}O$ values include -8.679 ‰, -8.960 ‰, -9.555 ‰ and -9.264 ‰ (Table 4a, Figure 4). As such, the rise and fall of isotope values do not systematically correspond. Therefore, the overall cyclicity of seasonal oscillations most likely represents environmentally-related shifts and only minimally reflects diagenetic alteration.

Strontium isotopes

Strontium was isolated from five specimens from the sampled outcrop, and $^{87}Sr/^{86}Sr$ measured with the Geochemical Laboratories VG-54 thermal ionization mass spectrometer (see Methods). The SRM 987 Sr isotope standard was measured three times during the analysis period and all values fell within the established long term range of

measurements in this laboratory (0.710235 +/- 0.000039 for 2σ). Samples JM-1-9 and JM-1-66 represent subtidal environments of deposition, while samples JM-1-33 and JM-1-44 characterize peritidal environments, and JM-1-75b was collected from a supratidal depositional environment. The lowest $^{87}Sr/^{86}Sr$ value of 0.70917 was recorded in peritidal sample JM-1-44; all others were slightly more radiogenic, though the overall range was small (Table 5).

The low value also corresponds to the sample with the smallest Rb correction, suggesting this is the most primary value for the outcrop insofar as the secondary input of ^{87}Sr (from the decay of ^{87}Rb) was inconsequential (Ebneth et al., 2001). The low $^{87}Sr/^{86}Sr$ value corresponds to an age of ~500 Ma according to previously published and radiometrically calibrated chemostratigraphic schemes (Montanez et al., 2000; Ebneth et al., 2001), which is just slightly lower than the known peak $^{87}Sr/^{86}Sr$ value of the Phanerozoic.

Carbon isotopes

The data reveals an overall trend towards more negative $\delta^{13}C$ values, and is likely related to the onset of the HERB event -- even though the entire excursion is not yet revealed. The high-resolution samples at the base of the section provide a 2 ‰ constraint on natural variations across the carbonate platform, including the effects of diagenesis on depositional carbon isotope abundances. As such, the high-resolution stratigraphy and corresponding isotopic analyses provide a stratigraphic test of values obtained throughout the entire sample set. Clearly, the negative $\delta^{13}C$ excursion falls outside of the natural variation demonstrated by the high-resolution sample set; and, the subtidal lithofacies consistently highlight the overall negative-trending isotopic signature upwards in the progression.

The few supratidal and peritidal beds intact up-section from the high-resolution set correspond with small-scale variations seen at the base of the outcrop (Figure 4; Table 1). Specifically, the anomalous massive, sandy limestone at 135.9m (#JM-2-8) records a positive $\delta^{13}C$ shift typical of the lower high-resolution stratigraphy. Also, three grainstone beds, two with some dolotimization, at closely-spaced intervals (249.7m, 255m, and 269.5 m for #'s JM-2-18, JM-2-19, and JM-2-20, respectively) demonstrate a temporary trend to more positive $\delta^{13}C$ values.

In order to determine the external reproducibility for the carbonate isotopes, I conducted two runs using most of the same samples as in the first. I then calculated the average $\delta^{13}C$ value of the standard for the runs completed, which results in 0.501 ‰ for Run 1(a, b) versus 0.761 ‰ for Run 2. The standard $\delta^{13}C$ deviation reveals for Runs 1(a, b) 0.036 ‰ (1σ) and 0.072 ‰ (2σ) versus 0.018 ‰ (1σ) and 0.036 ‰ (2σ) for Run 2. For $\delta^{18}O$, the average is -10.226 ‰ with 0.111 (1σ) and 0.222 (2σ) for Run 1 (a, b) while Run 2 returns with an average of -9.425 ‰, 0.031 ‰ (1σ) and 0.061 ‰ (2σ). Both a graph of the $\delta^{13}C$ and $\delta^{18}O$ values from the three runs and a table with the specific isotope data highlight the close correlation between the individual data sets (Table 3a and 3b; Fig. 3). The isotopic results of the samples using the IsoPrime mass spectrometer at the University of Maryland can, therefore, be stated with a high degree of confidence.

Error analysis for $\delta^{13}C$ of the standard carbonate (LL1) in Run 1a uncovers +/- 0.037‰ (1σ) and +/- 0.074‰ (2σ). Run 1b produces +/- 0.035‰ (1σ) and +/- 0.070‰ (2σ). Error analysis for $\delta^{18}O$ of the standard carbonate (LL1) in Run 1a

yields +/- 0.120‰ (1σ) and +/- 0.240‰ (2σ). Run 1b results in +/- 0.101‰ (1σ) and +/-0.202‰ for (2σ). Run 2 error analysis reveals +/- 0.018‰ (1σ) and +/- 0.036‰ (2σ) for $\delta^{13}C$. Error analysis for $\delta^{18}O$ shows +/- 0.033‰ (1σ) and +/- 0.066‰ (2σ). Run 3 yields +/- 0.026‰ (1σ) and +/- 0.052‰ (2σ) for $\delta^{13}C$, and +/- 0.072‰ (1σ), +/- 0.144‰ (2σ) for $\delta^{18}O$.

Sulfur isotopes

Although there is ~ 1‰ error in values obtained by the CF gas source Isoprime mass spectrometer, general observations can be made about the overall trend in the data. Specifically, the anomalous ^{34}S enrichment of +34‰ correlates to other structurally bound sulfate in Late Cambrian carbonates (Claypool et al., 1980; Strauss et al., 1997). Additionally, several samples taken from the Conococheague Carbonates in central Virginia contain organic-rich material as well as pyrite, implying poorly oxygenated waters with stratified deeper water (Saltzman et al., 2000). Restricted basins (like the island-arc formed by the Taconic Orogeny) and areas of upwelling assist in the development of a stratified, anoxic ocean, giving rise to global oceanic anoxia and subsequent organic deposition (Railsback et al., 1990), which further validates the positive sulfur anomaly recorded.

Suggestions for Future Work

1. The sulfur results, at present, are not publishable. Replicate sulfur analyses are required to confirm these initial measurements given that the data was obtained while the CF gas source Isoprime mass spectrometer was experiencing fluctuating technical problems.
2. External reproducibility of the trace sulfate extraction method needs to be demonstrated by analyzing a single sample multiple times.
3. Insofar as only the downward trend in carbon isotopes is revealed, further sampling upsection is warranted (to capture the entire extent of HERB excursion).
4. Sr and Rb concentrations in the carbonates need to be determined to further characterize these samples.
5. The age range of the conodont biozones reported in the literature should be recalculated based on newer radiometric determinations.
6. Once all the data has been compiled, a more integrated model of these biogeochemical anomalies may be possible.

Conclusions

Periods of mass extinction, as evidenced at the end of the Permian (Holser, 1989), have been associated with strong negative carbon isotopic anomalies in seawater proxies (Varni, 2002). Events of this type are referred to as Strangelove oceans (Kump, 1991) in that the anomalies suggest a significant loss of primary photosynthetic input into the deep ocean, which in turn causes chemical changes in the whole ocean. Mass extinction of animals, including several species of trilobites (Saltzman et al., 2000), possibly related to environmental changes and studied extensively by biogeochemists worldwide, abounds in the Cambrian.

The question is could there have been similar mass extinctions of primary photoautotrophs at this time, and might this be reflected in the HERB event?

The coupled C and S isotope anomalies during the HERB event may be explained by widespread global anoxia, which may result from a the concentration of continents at low- to mid-latitudes and hindered ocean circulation, and/or a marked decline in primary productivity, which would attenuate oxygen fluxes to the oceans and atmosphere. If so, anoxic oceans would facilitate the water column dominance of bacterial sulfate reducers, as seen in the present day Black Sea (Varni, 2002). Long term sulfate reduction would cause seawater alkalinity to become increasingly ^{13}C depleted (read negative $\delta^{13}C$ values in carbonates), and through the production of $H_2{}^{32}S$ and precipitation as Fe_2S (provided iron were readily available in the anoxic ocean) residual oceanic sulfate would become increasingly enriched in ^{34}S. This residual sulfate, provided the model applies, would then be incorporated as trace sulfate in the Conococheague carbonates.

Indeed, other models for carbonate alkalinity have been postulated and include dissolution of preexisting carbonate in the oceans or bacterial sulfate reducers in anoxic deep oceans fed by methane or other low molecular weight compounds (Varni, 2002). However, given the reaction $C_{106}H_{263}O_{110}N_{16}P + 53SO_4^{2-} \rightarrow 39CO_2 + 67HCO_3^- + 16NH_4^+ + HPO_4^{2-} + 53HS^- + 39H_2O$ and the results reported in the preceding research, alkalinity, with negative $\delta^{13}C$, and trace sulfate, with positive $\delta^{34}S$, might be explained (particularly if BSR entered the water column and dominated seawater chemistry).

The carbon and oxygen data together with the age constraint provided by the Sr analysis provide substantial evidence for a negative-trending excursion consistent with the late Cambrian HERB event. The high-resolution stratigraphy at the base of the outcrop provides a constraint on depositional and diagenetic values. Furthermore, the concentrations of the continents at low- to mid-latitudes, a warm global climate, and high sea level prior to the excursion all suggest that the Conococheague formed during a widespread oceanic anoxic event (OAE).

Acknowledgements

I owe tremendous gratitude to my advisor Dr. A. Jay Kaufman for his support, guidance, encouragement, humor, patience and determination. There are no words that can fill the time, space, money and energy he gave to me in completing my thesis. Forever and ever and ever, amen. I also owe many thanks to Craig Hebert for answering endless questions about laboratory procedures, for staying after dark one week before his dissertation to photograph my samples using CL photospectrometry, for carrying the sledge hammer on every field outing, and for filling me in on all the big and little things I needed to know, often urgently so. In the same vein, I would like to thank the Department of Geology at the University of Maryland, especially Sandy Romeo for making sure I could properly use the Xerox machine and always get into the labs and Chemistry building, Bill Minarik for offering to bring in his camera when I thought I wouldn't be able to take photos over Spring Break, Dorothy Brown and Ginnette Villeneuve for making sure the sediment trap in the Rock Cutting Room was properly emptied, Drs. Candela and Piccoli for making sure the thesis presentations proceeded without glitch, and Todd Kaworski for being the glue that kept everything together.

Special thanks also go to R.L. McDonald of Strasburg, VA, for allowing access to his farm for the purposes of this study. Not just that, but for allowing me, too, to witness for the first time the birth of a calf.

Thank you to my parents who never gave up through the ten years it has taken me to earn my degree. I'm almost there, Mom and Dad. Todd, I love you. I am proud to be your sister. I wouldn't be here without you. D-Train, tallulamoo. You rock.

References

Berger, W. H. and Vincent, E., 1986, Deep-Sea Carbonates: Reading the Carbon-Isotope Signal: Geologische Rundschau, v. 75, p. 249-269.

Brasier, M. D., 1993, Toward a Carbon Isotope Stratigraphy in Hailwood, E. A. and Kidd, R. B., eds., High Resolution Stratigraphy: Geological Society Special Publication 70, p. 341-350.

Brasier, M. D. and Sukhov, S. S., 1998, The Falling Amplitude of Carbon Isotopic Oscillations through the Lower to Middle Cambrian: Northern Siberia Data: Canadian Journal of Earth Sciences, v. 35, p. 353-373.

Canfield, D. E., 1991, Sulfate Reduction in Deep-Sea Sediments: American Journal of Science, v. 291, p. 177-188.

Claypool, G. E., Holser, W. T., Kaplan, I. R. and others, 1980, The Age Curves of Sulfur and Oxygen Isotopes in Marine Sulfate and Their Mutual Interpretation: Chemical Geology, v. 28, p. 190-210.

Demicco, R. V., 1983, Wavy and Lenticular-Bedded Carbonate Ribbon Rocks of the Upper Cambrian Conococheague Limestone, Central Appalachians: Journal of Sedimentary Petrology, v. 53, p. 1121-1132.

Ebneth, S., Shields, G. A., Veizer, J., Miller, J. F., and J. H. Shergold, 2001, High-Resolution Strontium Isotope Stratigraphy Across the Cambrian-Ordovician Transition: Geochimica Acta, v. 65, p. 2273-2292.

Glumac, B. and Walker, K. R., 1998, A Late Cambrian Positive Carbon-Isotope Excursion in the Southern Appalachians: Relation to Biostratigraphy, Sequence Stratigraphy, Environments of Deposition, and Diagenesis: Journal of Sedimentary Research, v. 68, p. 1212-1222.

Hemming, N. G., Meyers, W. J. and Grams, J.C., 1989, Cathodoluminescence in Diagenetic Calcites; the Role of Fe and Mn as Deduced from Electron Probe and Spectrophotometric Measurements: Journal of Sedimentary Petrology, v. 59, p. 404-411.

Habicht, K. S. and Canfield, D. E., 1996, Sulphur Isotope Fractionation in Modern Microbial Mats and the Evolution of the Sulphur Cycle: Nature, v. 382, p. 342-343.

Hennecke, E., Ill Luter, G. W., DE Lange, G. J. and Hoefs, J., 1997, Sulphur Speciation in Anoxic Hypersaline Sediments from the Eastern Mediterranean Sea: Geochimica et Cosmochimica Acta, v. 61, p. 307-321.

Holser, W. T., Schoenlaub, H-P., Attrep, M. Jr., Boeckelmann, K., Klein, P., Margaritz, M., Orth, C. J., Fenninger, K., Jenny, C., Kralik, M., Mauritsch, H., Pak, E., Schramm, J-M., Stattegger, K., and Schmoeller, R., 1989, A Unique Geochemical Record at the Permo/Triassic Boundary: Nature, v. 337, p. 39-44.

Kajiwara, Y., Yamakita, S., Ishida, K., Ishiga, H., and Imai, A., 1994, Development of a Largely Anoxic Stratified Ocean and its Temporary Massive Mixing at the Permian/Triassic Boundary Supported by the Sulfur Isotope Record: Palaeogeography, Palaeoclimatology, Palaeoecology, v. 111, p. 367-379.

Kaufman, A. J., Hayes, J. M., Knoll, A. H., and Germs, G. J. B., 1991, Isotopic Compositions of Carbonates and Organic Carbon from Upper Proterozoic Successions in Namibia: Stratigraphic Variation and the Effects of Diagenesis and Metamorphism: Precambrian Research, v. 49, p. 301-327.

Kaufman, A. J., Jacobsen, S. B. and Knoll, A. H., 1993, The Vendian Record of Sr and C Isotopic Variations in Seawater: Implications for Tectonics and Paleoclimate: Earth and Planetary Science Letters, v. 120, p. 409-430.

Knoll, A. H. and Caroll, S. B., 1999, Early Animal Evolution: Emerging Views from Comparative Biology and Geology: Science, v. 284, p. 2129-2136.

Koerschner, W. F. and Read, J. F., 1989, Field and Modeling Studies of Cambrian Carbonate Cycles, Virginia Appalachians: Journal of Sedimentary Petrology, v. 59, p. 654-687.

Kump, Lee R., 1989, Alternative Modeling Approaches to the Geochemical Cycles of Carbon, Sulfur, and Strontium Isotopes: American Journal of Science, v. 289, p. 390-410.

Kump, Lee R., 1991, Interpreting Carbon-Isotope Excursions: Strangelove Oceans: Geology, v. 19, p. 299-302.

Kump, L. R. and Arthur, M. A., 1999, Interpreting Carbon-Isotope Excursions: Carbonates and Organic Matter: Chemical Geology, v. 161, p. 181-198.

McDowell, Robert C., 1995, Preliminary Geologic Map of the Mountain Falls Quadrangle, Frederick and Shenandoah Counties, Virginia, and Hampshire County, West Virginia: USGS Open-file Report.

Montanez, I. P. and Read, J. F., 1992, Eustatic Control on Early Dolotimization of Cyclic Peritidal Carbonates: Evidence from the Early Ordovician Upper Knox Group, Appalachians: Geological Society of America Bulletin, v. 104, p. 872-886.

Montanez, I. P., Banner, J. L., Osleger, D. A., Borg, L. E., and Bosserman, P. J., 1996, Integrated Sr Isotope Variations and Sea-Level History of Middle to Upper

Cambrian Platform Carbonates: Implications for the Evolution of Cambrian Seawater $^{87}Sr/^{86}Sr$: Geology, v. 24, p. 917-920.

Montanez, I.P., Osleger, D.A., Banner, J. L., Mack, L. E., and Musgrove, M., 2000, Evolution of the Sr and C Isotope Composition of Cambrian Oceans: GSA Today, v. 10, p. 1-7.

Palmer, A. R., 1998, A Proposed Nomenclature for Stages and Series for the Cambrian of Laurentia: Canadian Journal of Earth Sciences, v. 35, p. 323-328.

Prothero, D. R. and Schwab, F., 1996, Sedimentary Geology: An Introduction to Sedimentary Rocks and Stratigraphy: W. H. Freeman and Company, New York.

Railsback, L. B., Ackerly, S. C., Anderson, T. F., and Cisne, J. L., 1990, Palaeontological and Isotope Evidence for Warm Saline Deep Waters in Ordovician Oceans: Nature, v. 343, p. 156-159.

Ripperdan, R., Magaritz, M., Nicoll, R. S. and Shergold, J. H., 1992, Simultaneous Changes in Carbon Isotopes, Sea Level, and Conodont Biozones within the Cambrian-Ordovician Boundary Interval at Black Mountain, Australia: Geology, v. 20, p. 1039-1042.

Ripperdan, R., 2002, The HERB Event: End of the Cambrian Carbon Cycle Paradigm?: GSA Denver Annual Meeting Abstract, Paper 184-3.

Ripperdan, R., 2002, Personal communication through Jay Kaufman by e-mail correspondence: Copy of letter available upon request.

Saltzman, M. R., Runnegar, B. and Lohmann, K. C., 1998, Carbon Isotope Stratigraphy of Upper Cambrian (Steptoean Stage) Sequences of the Eastern Great Basin: Record of a Global Oceanographic Event: Geological Society of America Bulletin, v. 110, p. 285-297.

Saltzman, M. R., Ripperdan, R. L., Brasier, M. D., Lohmann, K. C., Robinson, R. A., Chang, W. T., Peng, S., Ergaliev, E. K., and Runnegar, B. R., 2000, A Global Carbon Isotope Excursion (SPICE) During the Late Cambrian: Relation to Trilobite Extinctions, Organic-Matter Burial and Sea Level: Palaeogeography, Palaeoclimatology, Palaeoecology, v. 160, p. 211-223.

Strauss, Harald, 1997, The Isotopic Composition of Sedimentary Sulfur through Time: Palaeogeography, Palaeoclimatology, Palaeoecology, v. 132, p. 97-118.

Varni, Michael Anthony, 2002, The Sulfur Isotopic Composition of Structurally-Bound Sulfate in Neoproterozoic Carbonates: Implications for Sources of Alkalinity: Master's Dissertation, University of Maryland Department of Geology.

Veizer, J., Ala, D., Azmy, K., Bruckschen, P., Buhl, D., Bruhn, F., Carden, G. A., Diener, A, Ebneth, S., Godderis, Y., Jasper, T., Korte, C., Pawellek, F., Podlaha, O. G., and Strauss, H., 1999, $^{87}Sr/^{86}Sr$, $\delta^{13}C$ and $\delta^{18}O$ Evolution of Phanerozoic Seawater: Chemical Geology, v. 161, p. 59-88.

Wilde, P. and Berry, W. B. N., 1984, Destabilization of the Oceanic Density Structure and Its Significance to Marine "Extinction" Events: Palaeogeography, Palaeoclimatology, Palaeoecology, v. 48, p. 143-162.

Appendix

"I pledge on my honor that I have not given or received any unauthorized assistance or plagiarized on this assignment."

Ruth F. Thompson